# DNA damage–induced phosphorylation of CtIP at a conserved ATM/ATR site T855 promotes lymphomagenesis in mice

Xiaobin S. Wang[a,b], Demis Menolfi[a], Foon Wu-Baer[a], Marco Fangazio[a], Stefanie N. Meyer[a], Zhengping Shao[a], Yunyue Wang[a], Yimeng Zhu[a], Brian J. Lee[a], Verna M. Estes[a], Olivia M. Cupo[a], Jean Gautier[a,c], Laura Pasqualucci[a,d], Riccardo Dalla-Favera[a,c,d,e], Richard Baer[a,d], and Shan Zha[a,d,e,f,1]

[a]Institute for Cancer Genetics, Vagelos College for Physicians and Surgeons, Columbia University, New York City, NY 10032; [b]Graduate Program of Pathobiology and Molecular Medicine, Vagelos College for Physicians and Surgeons, Columbia University, New York, NY 10032; [c]Department of Genetics and Development, Vagelos College for Physicians and Surgeons, Columbia University, New York, NY 10032; [d]Department of Pathology and Cell Biology, Herbert Irving Comprehensive Cancer Center, Vagelos College for Physicians and Surgeons, Columbia University, New York, NY 10032; [e]Department of Immunology and Microbiology, Vagelos College for Physicians and Surgeons, Columbia University, New York, NY 10032; and [f]Division of Pediatric Hematology, Oncology and Stem Cell Transplantation, Department of Pediatrics, Vagelos College for Physicians and Surgeons, Columbia University, New York, NY 10032

Edited by Wei Yang, NIH, Bethesda, MD, and approved July 13, 2021 (received for review March 20, 2021)

**CtIP is a DNA end resection factor widely implicated in alternative end-joining (A-EJ)–mediated translocations in cell-based reporter systems. To address the physiological role of CtIP, an essential gene, in translocation-mediated lymphomagenesis, we introduced the T855A mutation at murine CtIP to nonhomologous end-joining and Tp53 double-deficient mice that routinely succumbed to lymphomas carrying A-EJ–mediated IgH-Myc translocations. T855 of CtIP is phosphorylated by ATM or ATR kinases upon DNA damage to promote end resection. Here, we reported that the T855A mutation of CtIP compromised the neonatal development of *Xrcc4*$^{-/-}$*Tp53*$^{-/-}$ mice and the IgH-Myc translocation-driven lymphomagenesis in *DNA-PKcs*$^{-/-}$*Tp53*$^{-/-}$ mice. Mechanistically, the T855A mutation limits DNA end resection length without affecting hairpin opening, translocation frequency, or fork stability. Meanwhile, after radiation, CtIP-T855A mutant cells showed a consistent decreased Chk1 phosphorylation and defects in the G2/M cell cycle checkpoint. Consistent with the role of T855A mutation in lymphomagenesis beyond translocation, the CtIP-T855A mutation also delays splenomegaly in λ-Myc mice. Collectively, our study revealed a role of CtIP-T855 phosphorylation in lymphomagenesis beyond A-EJ–mediated chromosomal translocation.**

CtIP | lymphomagenesis | DNA damage response | checkpoint | alternative end-joining

B cell lymphomas often carry oncogenic chromosomal translocations involving the immunoglobulin (Ig) genes, where programmed DNA double-strand breaks (DSBs) are created during the assembly and modifications of the Ig loci (1). The classical nonhomologous end-joining (cNHEJ) pathway of DSB repair is exclusively required for the assembly of functional Ig genes by V(D)J recombination. However, significant (up to 25 to 50%) class switch recombination (CSR) on the Ig heavy chain (IgH) can be achieved in cNHEJ-deficient cells via alternative end-joining (A-EJ), a distinct DSB repair pathway that preferentially uses microhomologies (MHs) at the junctions (2–6). In addition to CSR, the A-EJ pathway can also generate chromosomal translocations in reporter assays (7–9). DNA end resection that generates 3′ single-stranded DNA (ssDNA) overhangs (10) promotes A-EJ by exposing the flanking MHs. However, whether end resection is necessary for A-EJ–mediated oncogenic translocation and lymphomagenesis in vivo remains unknown.

The C-terminal–binding protein (CtBP)-interacting protein (CtIP), like its yeast ortholog Sae2, initiates DNA end resection together with the MRE11-RAD50-NBS1 (MRN) nuclease complex (11). By virtue of its resection activity, CtIP was implicated in A-EJ (7–9). CtIP expression and protein levels are higher in S and G2 phases and lower in the G1 phase (12, 13). Like the MRN complex, CtIP is essential for murine development (14) and the proliferation of normal lymphocytes (4, 15, 16), rendering it difficult to examine its role during oncogenesis using null or conditional-null alleles. CtIP is phosphorylated by CDK at T847 in the S and G2 phases of the cell cycle (17) and by ATM and ATR kinases at T859 (T855 in mouse) and other sites upon DNA damage (18–21). While T847 phosphorylation of CtIP is essential for murine development (16), mice carrying an alanine substitution at the T855 phosphorylation site of CtIP (*Ctip*$^{T855A}$) develop normally with mild end resection defects (4, 15). Moreover, *Ctip*$^{T855A/T855A}$ mice display normal lymphocyte development and proliferation (4, 15), providing a tool to test how CtIP and T855 phosphorylation contribute to chromosomal translocation and lymphomagenesis in vivo.

The *cNHEJ/Tp53* double-deficient mice routinely succumb to pro–B cell lymphomas bearing A-EJ–mediated IgH-Myc translocation and coamplification (22–24), providing an ideal model to examine the role of CtIP and end resection in A-EJ–mediated lymphomagenesis. Mechanistically, the initial translocation joins a RAG-initiated IgH DSB on chromosome 12 with sequences downstream of the *c-Myc* oncogene on chromosome 15 to form a

## Significance

Upon DNA damage, ATM and ATR kinase phosphorylate CtIP at T855 and several other sites. This study identified a physiological role of DNA damage–induced CtIP phosphorylation at T855 using mouse models. Specifically, we showed that while not affecting normal development and physiological DNA repair in developing lymphocytes, the T885A mutation of CtIP reduced the extent of DNA end resection, compromised the maintenance of the DNA damage–induced G2/M checkpoints, and delayed Myc-induced lymphomagenesis.

Author contributions: X.S.W., L.P., R.B., and S.Z. designed research; X.S.W., D.M., M.F., and S.N.M. performed research; X.S.W., F.W.-B., Z.S., Y.W., Y.Z., B.J.L., V.M.E., O.M.C., J.G., R.D.-F., and S.Z. contributed new reagents/analytic tools; X.S.W., D.M., M.F., S.N.M., L.P., and S.Z. analyzed data; X.S.W., R.B., and S.Z. wrote the paper; O.M.C. provided technical support for the animal colony; J.G. provided critical suggestions and discussion; R.D.-F. provided critical suggestion and reagents; and R.B. provided critical suggestions.

The authors declare no competing interest.

This article is a PNAS Direct Submission.



[1]To whom correspondence may be addressed. Email: sz2296@columbia.edu.

This article contains supporting information online at https://www.pnas.org/lookup/suppl/doi:10.1073/pnas.2105440118/-/DCSupplemental.

Published September 14, 2021.

dicentric (12, 15) chromosome (22). The dicentric intermediate breaks during mitosis, and the chromosome that contains the IgH-Myc translocation is joined with its sister to form a new dicentric chromosome, thereby initiating a breakage-fusion-bridge (BFB) cycle and eventually leading to a coamplification of IgH-Myc translocation under proliferation selection (1, 22). Since this occurs in cNHEJ-deficient cells, the initial translocation and the dicentric formation are both mediated by the A-EJ pathway. *Tp53* deficiency is critical for the tolerance of the genomic instability and subsequent overexpression of the *Myc* oncogene. In addition to *Xrcc4*/*Tp53*-deficient mice, other *cNHEJ*/*Tp53*-deficient models, including Artemis- and DNA-PKcs–deficient mice, also develop pro–B cell lymphomas with IgH-Myc coamplification (24–27), although the exact organization of amplicons remains undetermined. In addition to these experimental pro–B cell lymphoma models, BFB cycles also underlie tumor initiation and drug resistance in other human cancers (28, 29).

Here, we examine how CtIP-mediated end resection contributes to A-EJ–mediated chromosomal translocations and lymphomagenesis by characterizing cNHEJ/Tp53 double-deficient mice with or without the CtIP-T855A mutation. The results showed that the CtIP-T855A mutation causes neonatal lethality in $Xrcc4^{-/-}Tp53^{-/-}$ mice without apparent lymphomas or hematopoietic failure. Instead, the CtIP-T855A mutation exacerbates the reduced mitotic index in $Xrcc4^{-/-}Tp53^{-/-}$ olfactory neurons. In contrast, $CtIP^{T855A/T855A}Ku70^{-/-}$ mice are viable, although small even with wild-type (WT) *Tp53* status. Moreover, the CtIP-T855A mutation delays lymphomagenesis and alters the tumor spectrum of $DNA\text{-}PKcs^{-/-}Tp53^{-/-}$ mice. Yet, high-throughput genome-wide translocation sequencing (HTGTS) of RAG- and endonuclease-initiated DSBs shows that CtIP T855 phosphorylation is not required for hairpin opening or the initiation of end resection but consistently reduces the extent of end resection. Correspondingly, the CtIP-T855A mutation attenuates splenomegaly in the *λ-Myc* transgenic mouse model, suggesting a role for T855 phosphorylation in lymphomagenesis beyond translocation. In this context, $CtIP^{T855A/T855A}$ cells show no measurable defects in replication fork stability but consistent defects in IR-induced G2/M checkpoint maintenance.

## Results

**The CtIP-T855A Mutation Causes Neonatal Lethality in $Xrcc4^{-/-}Tp53^{-/-}$ Mice.** To elucidate the physiological functions of CtIP in lymphomagenesis, we introduced the CtIP-T855A mutation into $Xrcc4^{-/-}Tp53^{-/-}$ mice, which routinely succumb to pro–B cell lymphomas bearing an A-EJ–mediated IgH-Myc translocation and coamplification (22). $Xrcc4^{-/-}Tp53^{-/-}$ and $Xrcc4^{-/-}Tp53^{+/-}$ mice were small and were born at reduced rates (25), and the CtIP-T855A mutation did not further reduce the weight or the birth rate of $Xrcc4^{-/-}Tp53^{-/-}$ mice (Fig. 1*A* and *SI Appendix*, Fig. 1*A*). While control $Xrcc4^{-/-}Tp53^{-/-}$ mice succumbed to $B220^{+}IgM^{-}CD43^{+}$ pro–B cell lymphomas (*SI Appendix*, Fig. 1*B*) by ∼10 wk of age, all $CtIP^{T855A/T855A}Xrcc4^{-/-}Tp53^{-/-}$ ($n = 6$) and $CtIP^{T855A/T855A}Xrcc4^{-/-}Tp53^{+/-}$ ($n = 5$) mice died by 21 d of age without detectable lymphomas (Fig. 1*B*) (22, 25). The frequency of red blood cells, platelets, and hematopoietic stem and progenitor cells (Lin−Scal+cKit+) were comparable between the neonatal lethal $CtIP^{T855A/T855A}Xrcc4^{-/-}Tp53^{-/-}$ mice and the viable $Xrcc4^{-/-}Tp53^{-/-}$ mice (Fig. 1 *C* and *D* and *SI Appendix*, Fig. 1 *C–E*), excluding anemia or bone marrow failure as the cause for early lethality.

Xrcc4 loss causes Tp53-dependent postmitotic neuronal apoptosis (25). We thus examined whether the CtIP-T855A mutation further compromises neuronal development. Murine neurogenesis in the olfactory bulb continues after birth (30). On an $Xrcc4^{-/-}Tp53^{-/-}$ background, the CtIP-T855A mutation does not affect the proliferation index, as measured by Ki67+ staining (*SI Appendix*, Fig. 1*F*), or apoptosis, as measured by cleaved Caspase 3 staining (*SI Appendix*, Fig. 1*G*), of the olfactory neurons. Yet, both $Xrcc4^{-/-}Tp53^{-/-}$ and $CtIP^{T855A/T855A}Xrcc4^{-/-}Tp53^{-/-}$ mice accumulate large dark nuclei in the olfactory bulbs (Fig. 1*E*), consistent with G2 arrest and replication stress. Quantitatively, the levels of late G2 and mitotic nuclei (positive for phosphorylated Serine 10 of Histone H3, pH3+) were reduced in $Xrcc4^{-/-}Tp53^{-/-}$ mice ($P = 0.0021$) and further reduced in $CtIP^{T855A/T855A}Xrcc4^{-/-}Tp53^{-/-}$ mice ($P < 0.001$ versus WT and $P = 0.044$ versus $Xrcc4^{-/-}Tp53^{-/-}$) (Fig. 1*F*). There are three pH3 staining patterns: small puncta without pan-nuclear staining (type I, late G2 phase, purple), large nucleoli puncta with diffused nuclear staining (type II, early M phase/prophase, blue), and condensed dark staining (type III, M phase, red) (Fig. 1*G*). The T855A mutation markedly reduced the frequency of type II and type III (mitosis, $P < 0.0001$) nuclei in $Xrcc4^{-/-}Tp53^{-/-}$ mice, indicating G2/M arrest (Fig. 1*H*). Meanwhile, $CtIP^{T855A/T855A}Ku70^{-/-}$ mice with normal Tp53 were small but born alive and can survive beyond 21 d (Fig. 1*I* and *SI Appendix*, Fig. 1*H*), suggesting that CtIP-T855 phosphorylation might contribute to the processing of the KU blocked ends in cNHEJ-deficient cells.

**The CtIP-T855A Mutation Delays Lymphomagenesis in $DNA\text{-}PKcs^{-/-}Tp53^{-/-}$ Mice.** To circumvent neonatal lethality and study the impact of CtIP-mediated end resection on lymphomagenesis, we introduced the CtIP-T855A mutation into $DNA\text{-}PKcs^{-/-}Tp53^{-/-}$ mice, which also develop spontaneous pro–B cell lymphomas (26, 31, 32). Although the CtIP-T855A mutation did not affect the embryonic development or birth rate of $DNA\text{-}PKcs^{-/-}Tp53^{-/-}$ mice (*SI Appendix*, Fig. 2*A*), the overall survival of these mice was moderately extended (*SI Appendix*, Fig. 2*B*). Notably, the CtIP-T855A mutation reduced the frequency (from 94%, 28/33 to 68%, 17/25) and extended the latency (from $T_{1/2} = 73$ to 89 d) of pro–B cell lymphomas (B220+IgM−CD43+) in $DNA\text{-}PKcs^{-/-}Tp53^{-/-}$ mice (Fig. 2 *A–C* and *SI Appendix*, Fig. 2*C*). As a result, 32% (8 out of 25) of the $CtIP^{T855A/T855A}DNA\text{-}PKcs^{-/-}TP53^{-/-}$ mice succumbed to thymic lymphomas ($n = 5$), teratomas ($n = 2$), or sarcoma ($n = 1$) (Fig. 2*B*). The oncogenic translocations in the $DNA\text{-}PKcs^{-/-}Tp53^{-/-}$ pro–B cell lymphomas were not fully characterized. Fluorescent in situ hybridization (FISH) with probes specific for the IgH (Chr. 12) and c-Myc (Chr. 15) loci (33) revealed that 5/5 $DNA\text{-}PKcs^{-/-}Tp53^{-/-}$ and 4/5 $CtIP^{T855A/T855A}DNA\text{-}PKcs^{-/-}Tp53^{-/-}$ pro–B cell lymphomas contained clonal IgH-Myc translocations and coamplification (Fig. 2*D* and *SI Appendix*, Fig. 2*D*). One pro–B cell lymphoma sample from an older $CtIP^{T855A/T855A}DNA\text{-}PKcs^{-/-}Tp53^{-/-}$ mouse (143 d) with concurrent thymic lymphomas had an IgH-Myc translocation pattern consistent with a dicentric intermediate in about 59% of the metaphases analyzed (Fig. 2 *D*, *Lower Right* and *SI Appendix*, Fig. 2*D*). These data revealed that IgH-Myc translocation and coamplification drive lymphomagenesis in $DNA\text{-}PKcs^{-/-}Tp53^{-/-}$ mice and that the CtIP-T855A mutation delays pro–B cell lymphomagenesis in part by suppressing IgH-Myc coamplification.

**T855 Phosphorylation Promotes End Resection and Is Dispensable for Hairpin Opening.** To understand how the CtIP-T855A mutation delays B cell lymphomagenesis, we examined its impact on translocation initiation and amplification. To form the IgH-Myc translocation, the hairpin coding ends (CEs) at the IgH loci of DNA-PKcs–deficient B cells have to be opened (34, 35). Both the MRN and CtIP, as well as its yeast ortholog Sae2, were implicated in the hairpin opening (15, 36–38). To determine whether the CtIP-T855A mutation affects hairpin opening, we derived v-abl kinase–transformed $DNA\text{-}PKcs^{-/-}$ and $CtIP^{T855A/T855A}DNA\text{-}PKcs^{-/-}Tp53^{-/-}$ B cells that harbor the integrated V(D)J recombination

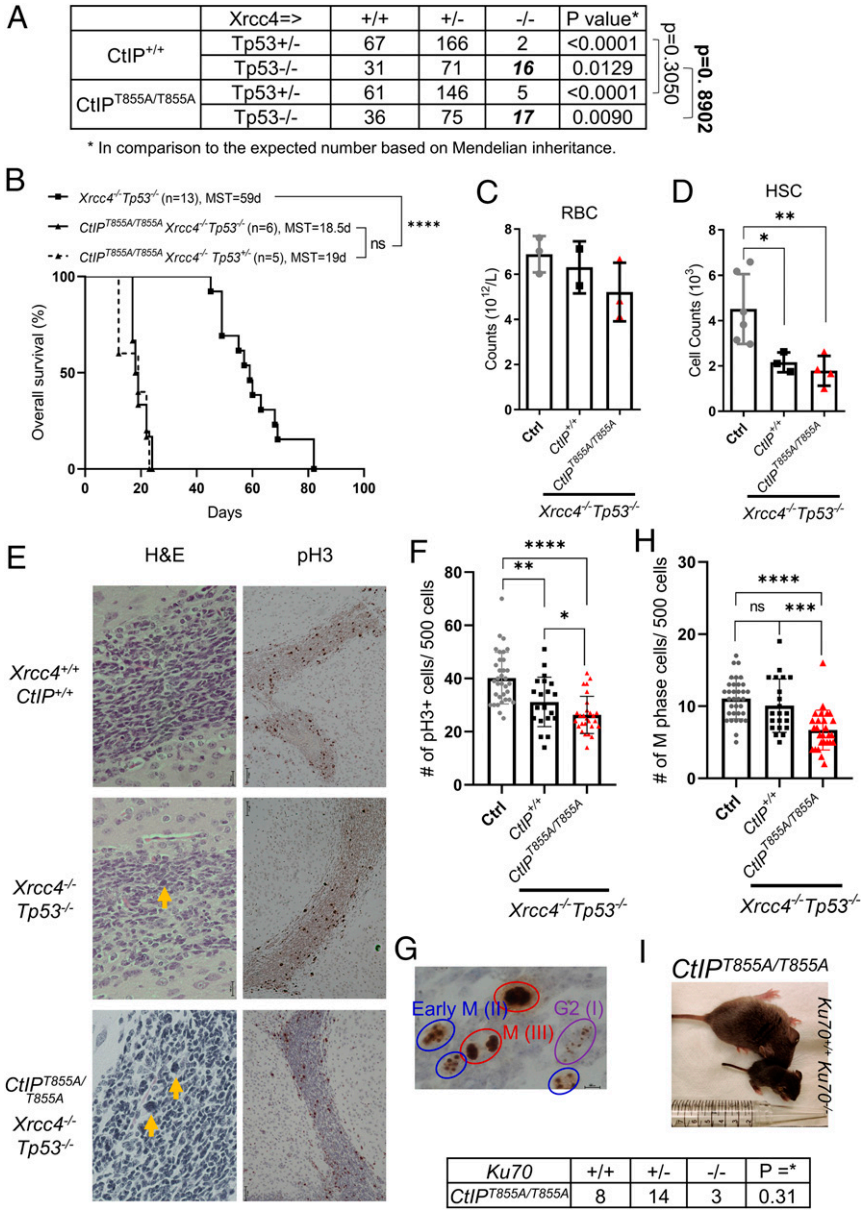


**Fig. 1.** Phosphorylation of CtIP at T855 is essential for the neonatal development of Xrcc4/Tp53 double-deficient mice. (*A*) The number of mice born from intercrossing between *Xrcc4*$^{+/-}$*TP53*-deficient mice. The *P* value was calculated via the $\chi^2$ test. (*B*) Kaplan–Meier survival curve of *CtIP*$^{T855A/T855A}$*Xrcc4*$^{-/-}$*Tp53*$^{-/-}$, *CtIP*$^{T855A/T855A}$*Xrcc4*$^{-/-}$*Tp53*$^{+/-}$, and *Xrcc4*$^{-/-}$*Tp53*$^{-/-}$ controls. Log-rank (Mantel–Cox) test, ****$P < 0.0001$; ns, not significant. (*C*) The concentration of red blood cells (RBC) in the peripheral blood of 16- to 19-d-old *CtIP*$^{T855A/T855A}$*Xrcc4*$^{-/-}$*Tp53*$^{-/-}$, *Xrcc4*$^{-/-}$*Tp53*$^{-/-}$, and WT controls. (*D*) Quantifications of bone marrow hematopoietic stem cells (HSC) (Lin−Sca1+cKit+); absolute counts per mouse. (*E*) Representative histological analyses of sagittal brain sectioning; enlarged cells with darkly stained nuclei are marked with orange arrows. (*F*) Frequency of pH3-positive cells per field. Mann–Whitney *U* test, *$P < 0.05$, **$P < 0.01$, ****$P < 0.0001$. (*G*) The representative image shows three types of pH3 staining patterns and their corresponding cell cycle stage. (*H*) Frequency of G2M and M phase cells per field. Mann–Whitney *U* test, ***$P < 0.001$, ****$P < 0.0001$. Quantifications in *F* and *H* were performed on data collected from five WT, four *Xrcc4*$^{-/-}$*Tp53*$^{-/-}$, and three *CtIP*$^{T855A/T855A}$*Xrcc4*$^{-/-}$*Tp53*$^{-/-}$ mice, with at least seven independent fields from each mouse. (*I*) (*Top*) A representative picture of a *CtIP*$^{T855A/T855A}$*Ku70*$^{-/-}$ mouse (*Lower*) and its *CtIP*$^{A/A}$*Ku70*$^{+/+}$ littermate (*Upper*). (*Bottom*) The number of mice born from intercrossing between *CtIP*$^{T855A/T855A}$*Ku70*$^{+/-}$ parents. The *P* value was calculated via the $\chi^2$ test.

substrate (pMX-INV) (Fig. 3*A*) (35, 39, 40). In these cells, the v-abl kinase inhibitor, STI571 (also called imatinib), induced efficient G1 arrest (Fig. 3*B* and *SI Appendix*, Fig. 3*A*) and RAG-initiated cleavage of the pMX-INV substrate (39). Since CtIP protein level and end resection activity increase significantly in the S and G2 phases of the cell cycle (12, 13), we also released the cells (wash away STI571) into the S/G2 phase (in the presence of CDK1 inhibitor Ro3306) after 12 h (Fig. 3 *B*, *b*) or 24 h (Fig. 3 *B*, *c*) of G1 arrest (Fig. 3*B* and *SI Appendix*, Fig. 3*A*). The levels of unrepaired CEs increased in G1-arrested *DNA-PKcs*$^{-/-}$ and *Ctip*$^{T855A/T855A}$*DNA-PKcs*$^{-/-}$ cells and decreased in the cells released to the S/G2, regardless of CtIP genotype (Fig. 3*C*). To determine whether CE hairpins are opened, we performed TdT ligation–mediated PCR in which TdT can only add polyA to the opened hairpin ends and not to the hairpin sealed ends (Fig. 3*A*). While TdT ligation–mediated PCR can readily amplify opened CEs in Xrcc4$^{-/-}$ cells, CEs from G1-arrested or -released *DNA-PKcs*$^{-/-}$ and *Ctip*$^{T855A/T855A}$*DNA-PKcs*$^{-/-}$ cells were not observed

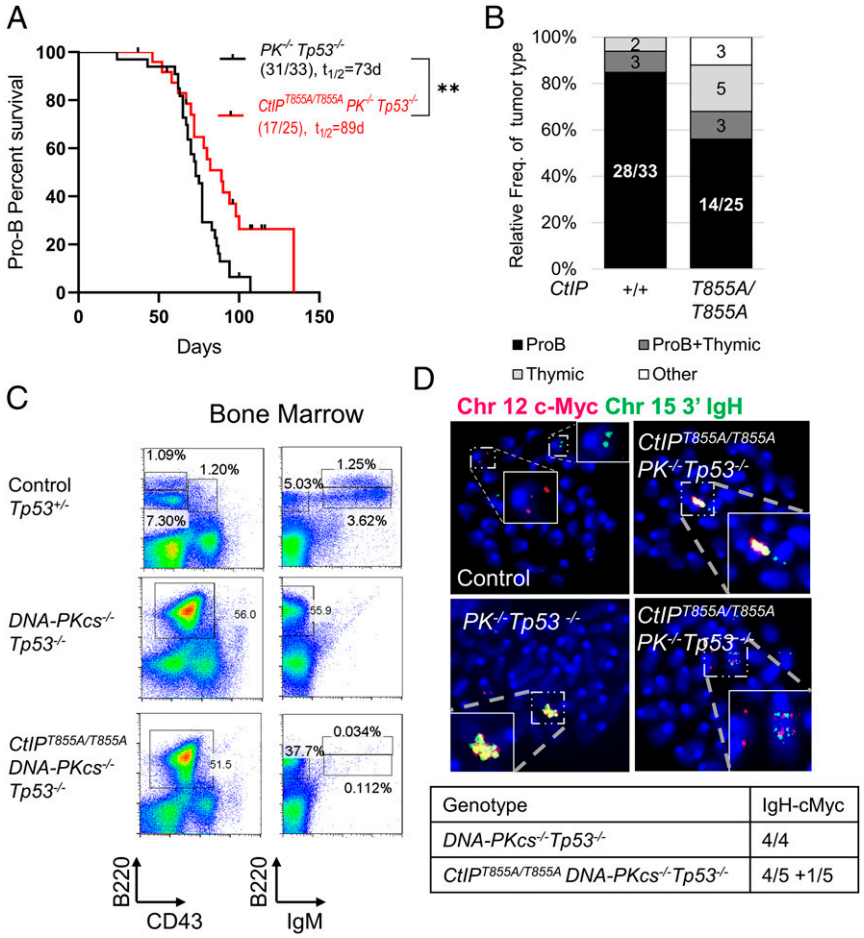


| Genotype | IgH-cMyc |
|---|---|
| *DNA-PKcs*$^{-/-}$*Tp53*$^{-/-}$ | 4/4 |
| *CtIP*$^{T855A/T855A}$ *DNA-PKcs*$^{-/-}$*Tp53*$^{-/-}$ | 4/5 +1/5 |

**Fig. 2.** CtIP-T855A mutation delays IgH-Myc–driven pro–B cell lymphomas and alters tumor spectrum in *DNA-PKcs*$^{-/-}$*Tp53*$^{-/-}$ mice. (*A*) Kaplan–Meier survival curve of *DNA-PKcs*$^{-/-}$*Tp53*$^{-/-}$ and *CtIP*$^{T855A/T855A}$*DNA-PKcs*$^{-/-}$*Tp53*$^{-/-}$ mice; the pro–B cell lymphoma only median survival of *DNA-PKcs*$^{-/-}$*Tp53*$^{-/-}$ mice is 73 d and of *CtIP*$^{T855A/T855A}$*DNA-PKcs*$^{-/-}$*Tp53*$^{-/-}$ mice is 89 d. Log-rank (Mantel–Cox) test, $^{**}P < 0.01$. (*B*) Tumor spectrum of *DNA-PKcs*$^{-/-}$*Tp53*$^{-/-}$ and *CtIP*$^{T855A/T855A}$*DNA-PKcs*$^{-/-}$*Tp53*$^{-/-}$ mice. (*C*) Representative flow cytometry analysis of bone marrow from a control mouse and *DNA-PKcs*$^{-/-}$*Tp53*$^{-/-}$ and *CtIP*$^{T855A/T855A}$*DNA-PKcs*$^{-/-}$*Tp53*$^{-/-}$ mice with pro–B cell lymphomas. (*D*) Representative FISH images from WT control samples (*Upper Left*), IgH-Myc translocations and coamplifications in lymphoma cells (spleen) from *DNA-PKcs*$^{-/-}$*Tp53*$^{-/-}$ mice (*Lower Left*) and from one *CtIP*$^{T855A/T855A}$*DNA-PKcs*$^{-/-}$*Tp53*$^{-/-}$ mouse with IgH-Myc coamplification (*Upper Right*) or one with dicentric intermediates (*Lower Right*). (*Bottom*) Quantifications of FISH analyses. Detailed quantification is shown in *SI Appendix*, Fig. 2*D*.

even after release to S/G2 (Fig. 3*D*). After being normalized to the available CEs (Fig. 3*C*), the CtIP-T855A mutation has no impact on the frequency of hairpin opening in DNA-PKcs–deficient B cells (Fig. 3*E*).

To compare the pattern of the hairpin opening between *DNA-PKcs*$^{-/-}$ and *CtIP*$^{T855A/T855A}$*DNA-PKcs*$^{-/-}$ cells, we employed HTGTS (41), a linear amplification–based sequencing method that can characterize thousands of junctions involving a specific DSB (the "bait" DSB). In this case, we chose the 5′ CE of the pMX-INV substrate as the bait (Fig. 3*A*). In WT and *CtIP*$^{T855A/T855A}$ cells, >80% of the DSB ends ("prey") that are joined with the 5′ CE fall within the pMX-INV V(D)J recombination substrate (Fig. 3*F*) and are almost all classical CJs with 3′ CEs (*SI Appendix*, Fig. 3*B*). Consistent with hairpin opening defects and increased chromosomal translocations, in *DNA-PKcs*$^{-/-}$ and *CtIP*$^{T855A/T855A}$*DNA-PKcs*$^{-/-}$ cells, only <40% of the prey breaks fall into the pMX-INV substrate (Fig. 3*F*). Nevertheless, >70% of junctions within the pMX-INV are with the 3′ CEs, with a moderate increase (3 to 6% to 8 to 10%) of inversions or hybrid join formation (with the 3′ signal ends) (*SI Appendix*, Fig. 3*B*). Moreover, the CJs recovered from both *DNA-PKcs*$^{-/-}$ and *CtIP*$^{T855A/T855A}$*DNA-PKcs*$^{-/-}$ cells have much longer deletions than those from WT and *CtIP*$^{T855A/T855A}$ cells (Fig. 3*G*). The CtIP-T855A mutation moderately reduced the mean deletion size from 47 to 36 base pairs (bp) in *DNA-PKcs*$^{-/-}$ cells (Fig. 3*G*). We next examined the bait 5′ CEs recovered from the junctions. In WT and *CtIP*$^{T855A/T855A}$ cells, ~70% of the hairpins opened at or around the apex (−2 to 4 bp), regardless of whether the cells were arrested in G1 (*SI Appendix*, Fig. 4*A*) or released to S/G2 (Fig. 3*I*). This pattern is consistent with the preferred cleavage sites of Artemis endonuclease in vitro (34, 42). While the junctions were broadly spread in *DNA-PKcs*$^{-/-}$ cells (Fig. 3*I*), the CtIP-T855A mutation limited hairpin opening to the region near the apex in *DNA-PKcs*$^{-/-}$ cells, especially in G2 (Fig. 3 *I*, *Bottom*). Finally, despite changes in hairpin opening hotspots, the CtIP T855A mutation does not affect the degree of microhomology (MH) in the CJ junctions recovered from *DNA-PKcs*$^{-/-}$ cells (Fig. 3*H*). Together, these data suggest that CtIP-T855 phosphorylation is not required for the initiation of end resection but may play a role in regulating the size of resection. Accordingly, spermatogenesis, which requires Sae2- and CtIP-initiated endonuclease cleavage of the Spo11 covalent complex by MRN-CtIP, is normal in *CtIP*$^{T855A/T855A}$ mice (*SI Appendix*, Fig. 4*B*).

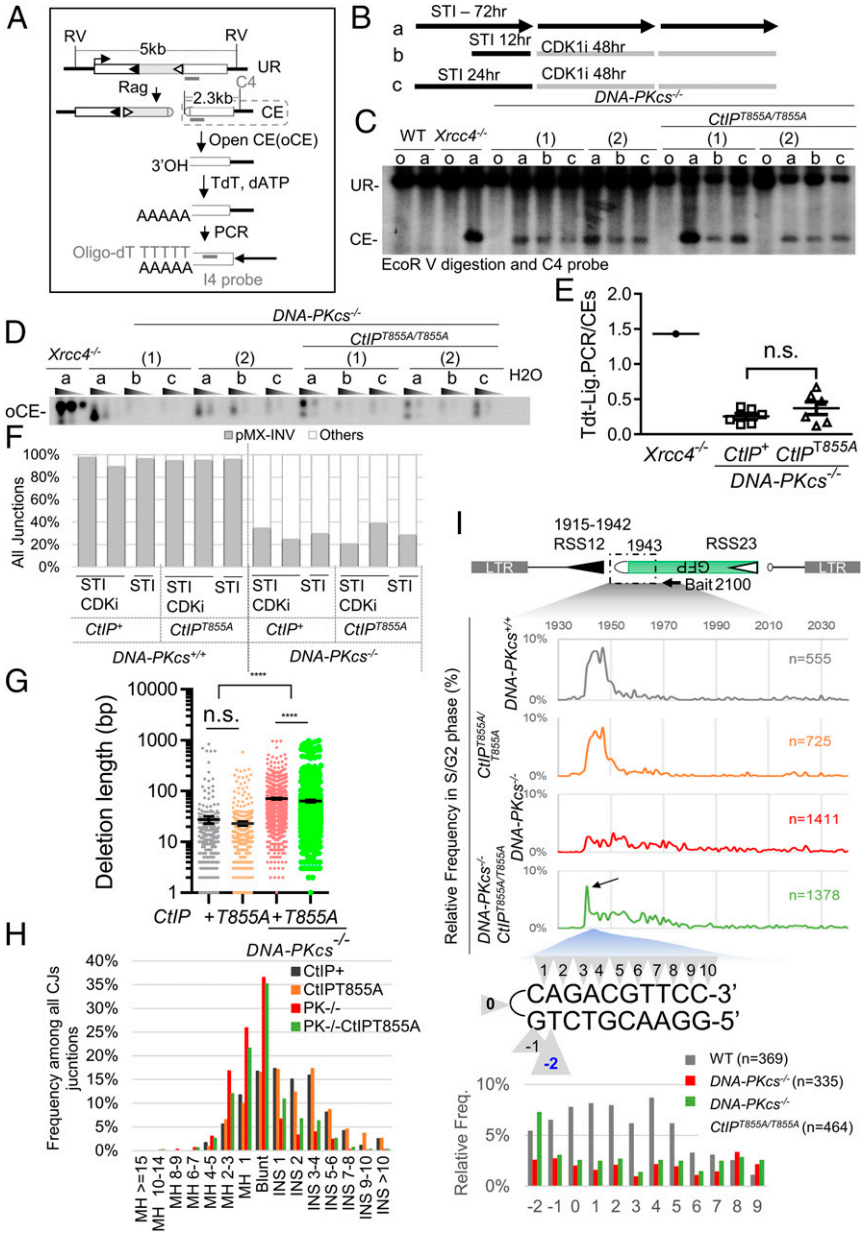


**Fig. 3.** CtIP-T855A mutation contributes to hairpin processing in *DNA-PKcs*$^{-/-}$ cells. (*A*) Schematic of pMX-INV substrate including the unrearranged (UR) and hairpin-sealed CE. The recombination signal sequences (RSS, triangles), I4 oligo probe, and C4 probe are marked. The opened hairpin structure can be detected by TdT-mediated ligation PCR. Briefly, TdT adds poly(A) to opened hairpin ends, which can be amplified with primers containing poly(T). Hairpinned ends cannot be amplified. (*B*) Workflow for experimental conditions used in *C*–*G*: v-abl–transformed B cells were arrested in G1 via STI571 (STI) treatment for 72 h (*a*), STI571 treated for 12 h (*b*) or 24 h (*c*) to induce RAG expression, and release to S/G2 phase with CDK1 inhibitor (Ro3306) for 48 h (*b* + *c*). (*C*) Southern blot of pMX-INV substrates using the scheme in *B*. UR, unrearranged, CE, coding ends, o: asynchronized (1) and (2) represent two biologically independent single clones. (*D*) Product of TdT-assisted PCR assays from multiple single clones with accumulated open ends from *Xrcc4*$^{-/-}$ cells as control. (*E*) The normalized relative intensity of TdT-mediated ligation PCR versus CE in *C*. The result of *Xrcc4*$^{-/-}$ cells was shown as the positive control. The Student's *t* test was used to calculate the *P* value, n.s., not significant. (*F*) Frequency of recovered HTGTS junctions mapped to within the pMX-INV substrate or elsewhere in the genome (others) from one G1 arrested sample (STI) and two independent repeats of G1 arrested and S/G2 released samples (STI → CDK1 inhibitor). (*G*) The distribution of total CJ deletion length (bp). Deletions from both sides of the breaks were added together. Extra-large deletions > 1,000 bp because of technical bias were removed. Mann–Whitney *U* test was used to calculate the *P* value. ****$P < 0.0001$; n.s., not significant. (*H*) The distribution of MH usage and insertion in all CJ recovered. (*I, Top)* Schematic diagram of pMX-INV substrate for V(D)J recombination with the location of the RSSs, the black arrow indicating the bait PCR primer starting position. (*Middle*) The footprint of hairpin-sealed CEs opening in the S/G2 phase, shown as the relative frequencies of the last aligned base pair on the bait end of the junctions with translocation patterns within the substrate. (*Bottom*) Diagrams of aligned bp locations and sequence at the CE, zoom-in frequency of the adjacent 12 bps around the opened hairpin end.

**T855 Phosphorylation Is Dispensable for Intersister Joining.** The next step of the BFB cycle is dicentric chromosome formation, a process that precedes the amplification of the IgH-Myc translocations (22). Concurrent breaks at both sister chromatids, like replicated broken dicentric chromosomes, may be joined together again to form another dicentric chromosome. This step is likely important for the amplification of the IgH-Myc translocation. Therefore, we asked whether the CtIP-T855A mutation

affects sister chromatid fusion by transducing v-abl cells with an inducible I-PpoI endonuclease (Fig. 4*A*) that recognizes 18 predicted cleavage sites in the mouse mm10 genome, plus one within each copy of the ribosomal DNA (rDNA) repeats (43) (*SI Appendix*, Fig. 4*C*). We then performed HTGTS using cleavage site no. 10 on chromosome 5 as the bait. In G1-arrested WT cells, ~20% of junctions involve preys that are local (at or around site 10), 25% involve other I-PpoI sites, and nearly 55% involve the rDNA repeats (Fig. 4*B*). The ~300 copies of rDNA in each murine cell likely contribute to the frequent involvement of rDNA. DNA-PKcs deficiency and S/G2 arrest both increase the frequency of local junctions (to 30 to 35%), with an additive effect in S/G2-arrested DNA-PKcs–deficient cells (nearly 50%) (Fig. 4*C*). The CtIP-T855A mutation does not significantly affect the overall distribution of prey breaks. Among the local deletional junctions, ~10% arise because of joining within the 4-bp overhang generated by I-PpoI (Fig. 4*D*). Consistent with cNHEJ deficiency, only <1% of the local junctions recovered from DNA-PKcs–deficient cells utilized the overhangs (Fig. 4*D*). Joining between sisters or with homologous chromosomes could generate a negative-strand junction (Fig. 4*A*, gray arrowheads), which increased in relative frequency in DNA-PKcs–deficient cells (Fig. 4*D*). The CtIP-T855A mutation moderately increased the frequency of negative-strand joining in DNA-PKcs–deficient cells. Given the overhang, most junctions recovered from WT or DNA-PKcs–deficient cells utilized 0 to 3 bp of MH, regardless of CtIP genotypes (*SI Appendix*, Fig. 5 *A* and *B*).

**T855 Phosphorylation of CtIP Plays a Role in G2/M Checkpoint Maintenance.** In addition to A-EJ, CtIP and Sae2 have also been implicated in checkpoint control (44–49). Specifically, resection by the CtIP/MRN complex can convert DSBs into ssDNA overhangs

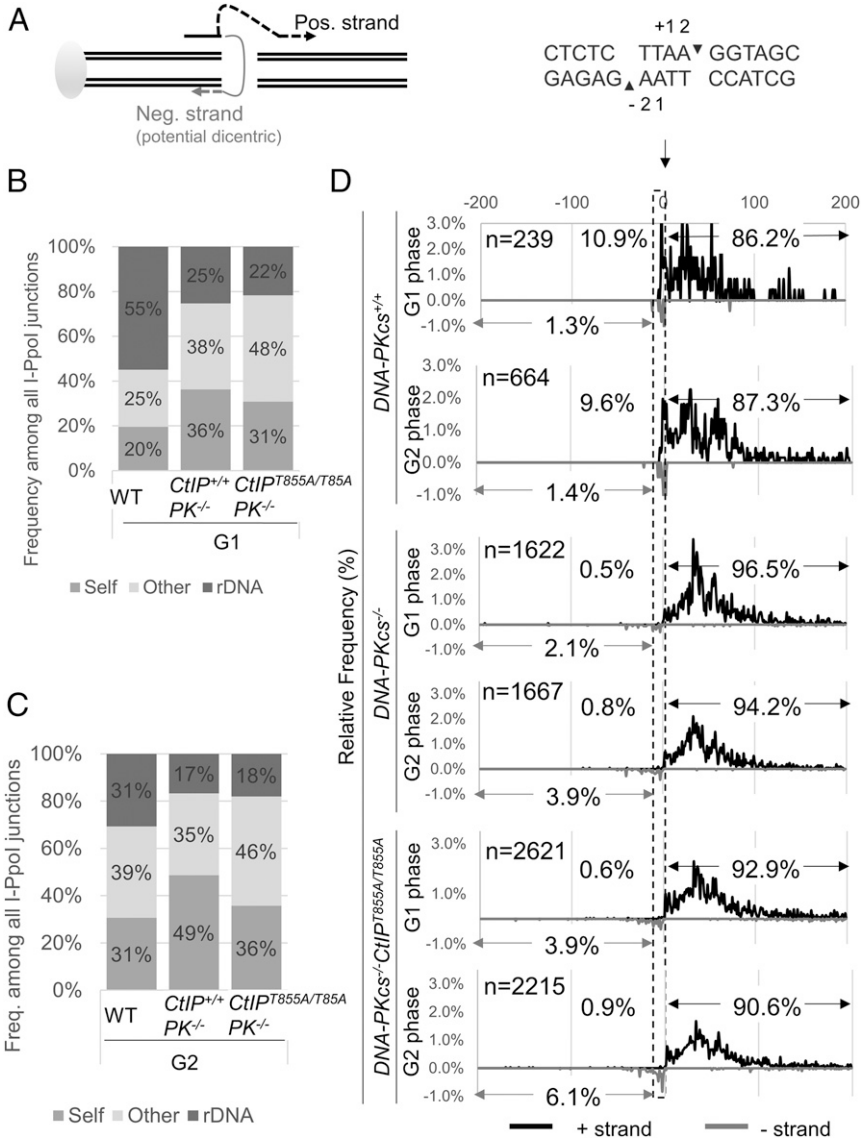


**Fig. 4.** CtIP-T855A mutation does not alter endonuclease-generated DSBs. (*A*) Scheme of translocations from I-PpoI-generated breaks, joining directions indicated with dashed arrows. (*B* and *C*) Relative frequency of junctions mapped to bait site (self), other I-PpoI sites (other), or rDNA region (rDNA) among all junctions in G1- (*B*) or G2- (*C*) arrested condition. (*D*) Relative distribution of local preys within + and – 200 bp from the cutting site in *DNA-PKcs*$^{-/-}$, and *CtIP*$^{T855A/T855A}$*DNA-PKcs*$^{-/-}$ v-abl–transformed B cells after 24-h I-PpoI induction in G1 phase or S/G2 phase. The frequencies of prey that fall into each region are indicated on each graph. With black traces indicating preys aligned to the + strand and gray traces indicating preys aligned to the – strand. (*Left*) −200 to −3 bp. (*Middle*) −2 to +2 bp sticky ends from enzyme cutting. (*Right*) +3 to +200 bp.

that can activate the ATR kinase (50). Given the relatively moderate effect of the T855A mutation on hairpin opening and translocation, we asked whether T855 phosphorylation plays a role in ionizing radiation (IR)-induced cell cycle checkpoint to accommodate oncogene-induced replication stress. To distinguish all four cell cycle phases, we costained the samples with the mitotic marker pH3, replication marker BrdU, and DNA content. Before IR, WT and $CtIP^{T855A/T855A}$ B cells showed similar patterns of cell cycle distribution (Fig. 5*A*). Three Gy IR induced a robust G2/M arrest in both WT and $CtIP^{T855A/T855A}$ B cells at 1 h. At 2 h after IR, significantly more $CtIP^{T855A/T855A}$ B cells entered mitosis than WT B cells (Fig. 5 *A* and *B*), suggesting that T855 phosphorylation might play a role in checkpoint maintenance. At 24 h after IR, WT cells showed a strong rebound of the mitotic index, which also occurred potentially to a less degree in $CtIP^{T855A/T855A}$ B cells (Fig. 5 *A* and *B*). Meanwhile, the IR-induced G1/S checkpoint measured by the BrdU+%/G1 phase was not affected by the CtIP-T855A mutation (Fig. 5*C*). Western blot analyses of radiated primary and immortalized B cells showed reduced phosphorylation of the ATR substrate Chk1 and marker for ssDNA—phosphorylated RPA in $CtIP^{T855A/T855A}$ cells (Fig. 5 *D* and *E*). Based on these data, we propose that CtIP phosphorylation at T855 promotes end resection, late-stage ATR activation, and G2/M checkpoint maintenance.

**The CtIP-T855A Mutation Delays MYC-Driven Splenomegaly.** If CtIP phosphorylation at T855 has a role in lymphomagenesis beyond translocation, then we expected the CtIP-T855A mutation to delay lymphomagenesis in the λ-Myc transgenic mouse model that develops spontaneous splenomegaly and carries the translocation in the germline (51). First, we somatically inactivated CtIP in $\lambda\text{-}Myc^{+}$ mice using B cell–specific $CD19^{Cre}$ (52) and the $CtIP^{co}$ conditional allele (16). However, no difference in overall survival, spleen weight, or immunophenotypes (including CD93,

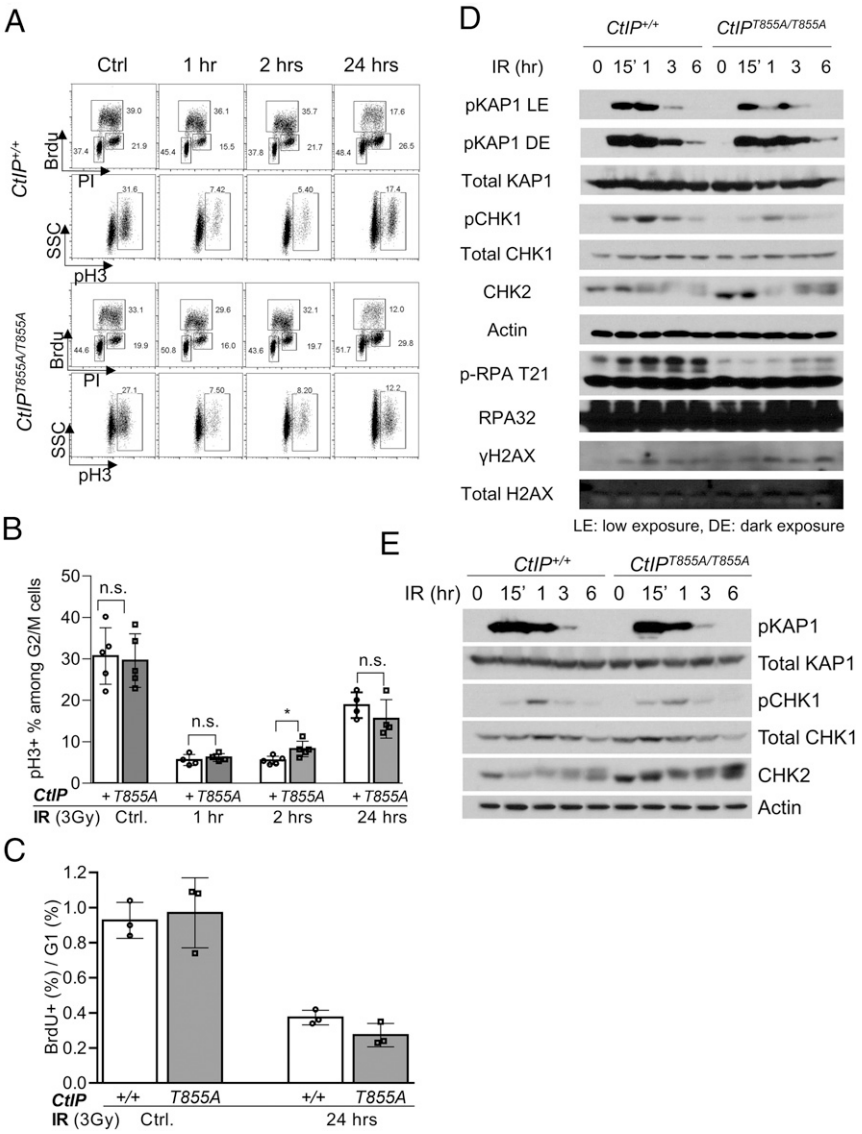


**Fig. 5.** Phosphorylation of CtIP at T855 contributes to G2/M checkpoint maintenance. (*A*) Representative flow cytometry analyses of the cell cycle with BrdU/PI and the percentage of pHistone3 Ser10-positive population within $BrdU^{-}$G2/M subpopulations in $CtIP^{+/+}$ and $CtIP^{T855A/T855A}$ primary B cells before and recovery after 3 Gy IR at 1, 2, and 24 h. (*B*) Quantifications of positive pHistone3 Ser10 percentage within $BrdU^{-}$G2/M populations from five independent experiments. Mann–Whitney *U* test, $^{*}P < 0.05$, n.s.: not significant, $P > 0.05$. (*C*) Quantifications of BrdU+ cells versus G1 cells from four different experiments. (*D* and *E*) Western blotting analyses of $CtIP^{+/+}$ and $CtIP^{T855A/T855A}$ primary B cells (*D*) or v-abl cell lines (*E*) before or after IR 3 Gy (B cells) or 10 Gy (v-abl cells).

which distinguishes relatively immature transitional B cells) were noted among the λ-*Myc*$^{+}$ mice regardless of CtIP genotype (*CD19*$^{Cre+}$*CtIP*$^{+/+}$, *CD19*$^{Cre+}$*CtIP*$^{co/+}$, or *CD19*$^{Cre+}$*CtIP*$^{co/co}$) (Fig. 6 *A* and *B* and *SI Appendix*, Fig. 5*C*). Of note, while CtIP was efficiently inactivated in the tumors arising in *CD19*$^{Cre+}$*CtIP*$^{co/+}$ mice (Fig. 6*C*, T2 to T4), lymphomas from *CD19*$^{Cre+}$*CtIP*$^{co/co}$ mice retained significant *CtIP*$^{co}$ alleles (Fig. 6*C*), suggesting the presence of escapers from the homozygous *CtIP* deletion. Therefore, we tested whether the germline CtIP T855A mutation affected Myc-driven lymphomagenesis by comparing *CtIP*$^{T855A/T855A}$λ-*Myc*$^{+}$ and control λ-*Myc*$^{+}$ mice. At 100 d of age, 73% (8/11) of λ-*Myc*$^{+}$ mice had splenomegaly as defined by >5.35 ‰ spleen/body weight ratio (99.7% CI of that of control WT mice of the same age) (Fig. 6*D*). In contrast, only 20% (2/10) of *CtIP*$^{T855A/T855A}$λ-*Myc*$^{+}$ mice developed splenomegaly at the same age (Fig. 6*D*). Flow cytometry analyses revealed 82% of

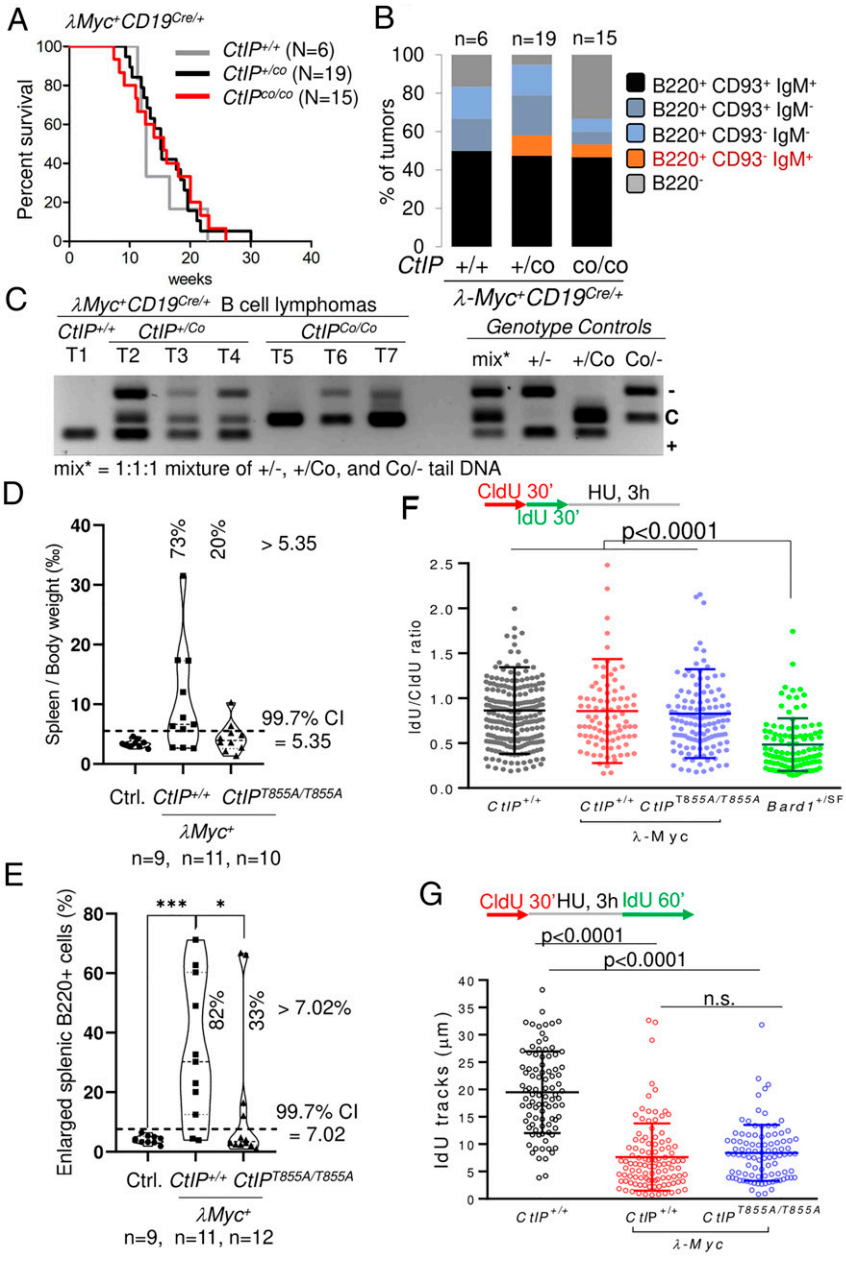


**Fig. 6.** CtIP-T855A mutation delays lymphomagenesis in the λ-Myc mouse model. (*A*) Kaplan–Meier survival curve for *CD19*$^{cre/+}$λ-*Myc*$^{+}$ *CtIP*$^{+/+}$, *CD19*$^{cre/+}$ λ-*Myc*+ *CtIP*$^{+/co}$, and *CD19*$^{cre/+}$λ-*Myc*$^{+}$*CtIP*$^{co/co}$ mice. (*B*) Phenotypic features of tumors developing in the spleen and/or lymph nodes of λ-Myc-CtIP compound mice. The positivity for the CD93 (also called AA4.1) marker identifies tumors originating from a transitional/immature B cell as opposed to tumors derived from mature B cells. (*C*) Representative PCR genotyping of *CtIP* in enlarged splenic cells. (*D*) Per-mille spleen weight (g)/body weight (g) among WT Ctrl ($n = 9$), λ-*Myc*$^{+}$ ($n = 11$), and *CtIP*$^{T855A/T855A}$λ-*Myc*$^{+}$ ($n = 10$) mice. The 99.7% CI calculated from the WT Ctrl group is marked on the graph. (*E*) Percentage of enlarged splenic B cells, calculated using the percentage of B220+ splenic cells multiplied by the percentage of the gate with the largest size (indicated in *B*). Mann–Whitney *U* test, *$P < 0.05$; ***$P < 0.001$. (*F*) Cytokine-activated primary B cells of indicated genotypes were pulse labeled with CldU for 30 min, then with IdU for 30 min, and then treated with 2 mM Hydroxyurea (HU) for 3 h before DNA fiber spreading. IdU/CldU ratio was calculated and plotted. Statistical analyses were carried out using GraphPad Prism and the Mann–Whitney *U* test. (*G*) Cytokine-activated primary B cells of indicated genotypes were pulse labeled with CldU for 30 min, treated with 2 mM HU for 3 h, and then puls -labeled with IdU for 1 h before DNA fiber spreading. The length of IdU fibers was measured and plotted. Statistical analyses were carried out using GraphPad Prism and the Mann–Whitney *U* test, n.s., not significant.

$\lambda$-$Myc^+$ mice showed enlarged B cells in the spleen in contrast to 33% in $CtIP^{T855A/T855A}$$\lambda$-$Myc^+$ mice (Fig. 6*E*). Given the role of Myc in replication stress response (53), we asked whether the CtIP-T855A mutation affects replication fork stability (Fig. 6*F*) or replication fork recovery after genotoxic challenges (Fig. 6*G*). The results showed that Myc-overexpressing B cells have a significant delay in recovery from HU-induced replication damage (Fig. 6*G*), yet the CtIP-T855A mutation does not measurably affect fork protection (Fig. 6 *F* and *G*). These data imply a role for CtIP T855 phosphorylation in supporting Myc-driven lymphomagenesis beyond translocation.

## Discussion

The A-EJ pathway and the related MH-mediated end-joining pathway have been implicated in the formation of chromosomal translocations. Although DNA end resection is thought to promote A-EJ, whether and how end resection contributes to A-EJ–mediated lymphomagenesis remains elusive. Here, we show, although dispensable for normal murine development, the phosphorylation of CtIP at T855 is critical for neonatal development of $Xrcc4^{-/-}Tp53^{-/-}$ mice. Moreover, the CtIP-T855A mutation delays lymphomagenesis in $DNA\text{-}PKcs^{-/-}Tp53^{-/-}$ mice. Yet, we failed to find consistent and measurable defects in the hairpin opening, sister chromatid ligation, and joint sequence formation in $CtIP^{T855A/T855A}DNA\text{-}PKcs^{-/-}$ cells in comparison to the $DNA\text{-}PKcs^{-/-}$ controls. Instead, we noted that 4/5 $CtIP^{T855A/T855A}DNA\text{-}PKcs^{-/-}Tp53^{-/-}$ B cell lymphomas carried amplified IgH-Myc translocations, suggesting that the T855A mutation does not prevent the initial translocation or the subsequent IgH-Myc amplification. HTGTS analyses documented moderately reduced end resection and a shift in hairpin opening position in $CtIP^{T855A/T855A}DNA\text{-}PKcs^{-/-}$ cells. Moreover, the *T855A* mutation delays lymphomas in the λ-Myc transgenic mice, indicating a role of T855 phosphorylation in lymphomagenesis beyond translocation. Taken together, the result is consistent with a selective role of T855 phosphorylation under stress conditions (e.g., IR or oncogene induced).

How does CtIP-T855 phosphorylation promote the neonatal development of $Xrcc4^{-/-}Tp53^{-/-}$ mice? In early studies, we and others have found that CtIP promotes end resection at DSBs accumulated in cNHEJ-deficient cells (4, 54), suggesting CtIP-mediated resection might represent a salvage pathway of DSB repair in $Xrcc4^{-/-}Tp53^{-/-}$ cells. This need for CtIP in end resection is in part due to the presence of KU, which prevents Exo1-mediated extensive end resection (55, 56). Consistent with this model, $CtIP^{T855A/T855A}Ku70^{-/-}$ mice, although small, are viable even in the presence of Tp53 (Fig. 1*I* and *SI Appendix*, Fig. 1*H*). While the CtIP-T855A mutation also reduces end resection in $DNA\text{-}PKcs^{-/-}$ cells (Fig. 3 *G* and *I*), the residual cNHEJ activity in $DNA\text{-}PKcs^{-/-}$ mice seems sufficient for embryonic and neonatal development. In this context, the normal meiosis and the unchanged frequency of translocations outside the pMX-INV substrates in $CtIP^{T855A/T855A}$ cells suggest that T855 phosphorylation is not required for the initiation of end resection but likely plays a role in the progression of end resection. In this regard, the chromatin retention of human CtIP is enhanced by phosphorylation of the corresponding residue (T859) (18), which may, in turn, promote the processability of end resection.

If T855 phosphorylation is not required for the hairpin opening and subsequent initial translocations and amplification, how does the T855A mutation delay lymphomagenesis? Four pieces of evidence suggest a translocation-independent role, perhaps through checkpoint regulation, although other pathways cannot be excluded. First, the T855A mutation suppressed lymphomagenesis of $\lambda$-$Myc^+$ mice that already carry an oncogenic transgene. Second, Myc overexpression has been linked to oncogene-induced replication stress, which often requires ATR kinase to be tolerant (57). Third, the CtIP-T855A mutation does not have a measurable role in replication fork stability or recovery in B cells, although Myc overexpression compromised replication fork recovery. Fourth, $CtIP^{T855A/T855A}$ B cells cannot generate ssDNA robustly, displaying reduced ATR activation (15). ATR plays a critical role in regulating replication fork stability, progression, and dormant origin firing that cannot be carried out by the ATM kinase (58). Mechanistically, CtIP and Sae2 can antagonize MRN- (or MRX in yeast) mediated checkpoint activation. In mammalian cells at an early time point (2 h), the CtIP T855A mutation mainly reduced ATR activation (11, 46, 48). In yeast, and at a later timepoint (~24 h), Sae2 limits persistent Rad53 activation by removing MRX and antagonizing Rad9 (44, 45, 49). The timing and cell type functional division between ATM (Tel1 in yeast) and ATR (Mec1 in yeast) may both contribute to this difference. We note the defects in maintaining the G2/M checkpoint in other WT cells are not in conflict with the reduced mitotic index in $CtIP^{T855A/T855A}Xrcc4^{-/-}Tp53^{-/-}$ mice since the accumulated breaks in $Xrcc4^{-/-}Tp53^{-/-}$ neurons have significantly reduced mitotic index.

In summary, our data identify two in vivo functions of CtIP-T855 phosphorylation—the escape from cNHEJ failure by promoting end resection and the enforcement of G2/M checkpoints under replication stress. We showed that ATM/ATR-mediated phosphorylation of CtIP at T855, while dispensable for normal development, is required in Xrcc4-deficient cells and during Myc-induced lymphomagenesis. These findings may explain why CtIP is amplified in a subset of gastric cancers (59). The translocation-independent function of CtIP in tumorigenesis highlights the important role of CtIP in linking DNA repair with cell cycle checkpoint and replication timing. CtIP is extensively modified during the S phase and in response to DNA damage. Our findings suggest that oncogenic stress or cNHEJ deficiency may underlie the physiological functions of other ATM/ATR- or CDK-mediated phosphorylation events as well as other post-translational modifications of CtIP, including the S327 phosphorylation that is also dispensable for murine development (16, 60).

## Materials and Methods

**Mice.** $CtIP^{T855A}$ (4, 15), $Xrcc4^{-/-}$ (25), $DNA\text{-}PKcs^{-/-}$ (61), $p53^{-/-}$ (62), $CD19^{Cre}$ (52), λ-*Myc* (63), and $CtIP^{Co}$ (60) mice were previously described. Mice in the $Xrcc4^{-/-}Tp53^{-/-}$ or $DNA\text{-}PKcs^{-/-}Tp53^{-/-}$ cohorts were aged until they showed clear signs of tumor and/or discomfort and then euthanized. $CtIP^{T855A/T855A}$ mice were crossed with λ-*Myc*+ mice and were analyzed at 100 d of age. Bone marrow, spleen, lymph nodes, and thymus were analyzed by flow cytometry as previously described (64, 65), and tissue was collected for further analysis. All animal works were conducted in a specific pathogen-free facility and had been approved by the Institutional Animal Care and Use Committee at Columbia University Medical Center. Flow cytometry was performed on a FACS Calibur (BD Bioscience), LSR II (BD Bioscience), or an Attune NxT flow cytometer (Thermo Fisher Scientific). See *SI Appendix* for a detailed antibody list.

**FISH.** Samples harvested from mice with enlarged spleens or lymph nodes were cultured in Roswell Park Memorial Institute medium with 100 ng/mL colcemid (Gibco 15212-012) for 4 h and harvested for metaphase analysis. Standard two-color FISH was performed with BAC199 as the *Igh* locus probe and BAC RP23-307D14 as the *c-myc* locus probe (33). The *Igh* probe was first labeled with biotin (Invitrogen 18047-015) and then blotted with Avidin-FITC (Sigma A2901). The *c-myc* probe was labeled with digoxigenin (DIG) (Roche 11745816910) and DyLight 594 goat anti-Dig (Vector DI-7594-0.5) as the secondary antibody for visualization. Images were acquired using ZEISS Imager Z2 and Metafer 4 system. Around 15 to 50 metaphases were analyzed for each tumor sample.

**Data Availability.** All study data are included in the article and/or *SI Appendix*.

**ACKNOWLEDGMENTS.** We thank Dr. Anna Lasorella at the Institute for Cancer Genetics for helping with the olfactory neuron analyses and the members of the S.Z. laboratory for discussion. We thank Mr. Tongwei Mo and Mrs. Hongyan Tang for mouse husbandry and tissue processing, respectively. We also wish to thank Mr. Federico Grullon for helping with the *λ-Myc*$^{+}$*CD19-Cre*$^{+}$*CtIP*$^{co/co}$ cohorts. This work was supported in part by NIH R01CA158073, R01CA215067, and R01CA226852 to S.Z.; 1P01CA174653 to R.B., S.Z., R.D., and J.G.; NIH R01CA172272 to R.B.; and NIH R35 CA197606 to J.G. X.W. was in part supported by Clinical and Translational Sciences Awards/NIH TL1 TR000082. D.M. was a Leukemia & Lymphoma Special Fellow. Y.Z. is a Cancer Research Institute Fellow. S.Z. was a Leukemia Lymphoma Society Scholar. This research used the flow cytometry and molecular cytogenetic shared resources funded through the NIH/National Cancer Institute Cancer Center Support Grant P30CA013696 to the Herbert Irving Comprehensive Cancer Center of Columbia University.

1. A. Nussenzweig, M. C. Nussenzweig, Origin of chromosomal translocations in lymphoid cancer. *Cell* **141**, 27–38 (2010).
2. C. T. Yan *et al*., IgH class switching and translocations use a robust non-classical end-joining pathway. *Nature* **449**, 478–482 (2007).
3. C. Boboila *et al*., Alternative end-joining catalyzes class switch recombination in the absence of both Ku70 and DNA ligase 4. *J. Exp. Med.* **207**, 417–427 (2010).
4. X. S. Wang *et al*., CtIP-mediated DNA resection is dispensable for IgH class switch recombination by alternative end-joining. *Proc. Natl. Acad. Sci. U.S.A.* **117**, 25700–25711 (2020).
5. J. L. Crowe *et al*., DNA-PKcs phosphorylation at the T2609 cluster alters the repair pathway choice during immunoglobulin class switch recombination. *Proc. Natl. Acad. Sci. U.S.A.* **117**, 22953–22961 (2020).
6. J. L. Crowe *et al*., Kinase-dependent structural role of DNA-PKcs during immunoglobulin class switch recombination. *Proc. Natl. Acad. Sci. U.S.A.* **115**, 8615–8620 (2018).
7. N. Bennardo, A. Cheng, N. Huang, J. M. Stark, Alternative-NHEJ is a mechanistically distinct pathway of mammalian chromosome break repair. *PLoS Genet.* **4**, e1000110 (2008).
8. Y. Zhang, M. Jasin, An essential role for CtIP in chromosomal translocation formation through an alternative end-joining pathway. *Nat. Struct. Mol. Biol.* **18**, 80–84 (2011).
9. C. Boboila *et al*., Alternative end-joining catalyzes robust IgH locus deletions and translocations in the combined absence of ligase 4 and Ku70. *Proc. Natl. Acad. Sci. U.S.A.* **107**, 3034–3039 (2010).
10. L. S. Symington, J. Gautier, Double-strand break end resection and repair pathway choice. *Annu. Rev. Genet.* **45**, 247–271 (2011).
11. A. A. Sartori *et al*., Human CtIP promotes DNA end resection. *Nature* **450**, 509–514 (2007).
12. O. Limbo *et al*., Ctp1 is a cell-cycle-regulated protein that functions with Mre11 complex to control double-strand break repair by homologous recombination. *Mol. Cell* **28**, 134–146 (2007).
13. X. Yu, R. Baer, Nuclear localization and cell cycle-specific expression of CtIP, a protein that associates with the BRCA1 tumor suppressor. *J. Biol. Chem.* **275**, 18541–18549 (2000).
14. P. L. Chen *et al*., Inactivation of CtIP leads to early embryonic lethality mediated by G1 restraint and to tumorigenesis by haploid insufficiency. *Mol. Cell. Biol.* **25**, 3535–3542 (2005).
15. X. Liu *et al*., CtIP is essential for early B cell proliferation and development in mice. *J. Exp. Med.* **216**, 1648–1663 (2019).
16. F. Polato *et al*., CtIP-mediated resection is essential for viability and can operate independently of BRCA1. *J. Exp. Med.* **211**, 1027–1036 (2014).
17. P. Huertas, F. Cortés-Ledesma, A. A. Sartori, A. Aguilera, S. P. Jackson, CDK targets Sae2 to control DNA-end resection and homologous recombination. *Nature* **455**, 689–692 (2008).
18. S. E. Peterson *et al*., Activation of DSB processing requires phosphorylation of CtIP by ATR. *Mol. Cell* **49**, 657–667 (2012).
19. N. Makharashvili *et al*., Catalytic and noncatalytic roles of the CtIP endonuclease in double-strand break end resection. *Mol. Cell* **54**, 1022–1033 (2014).
20. H. Wang *et al*., The interaction of CtIP and Nbs1 connects CDK and ATM to regulate HR-mediated double-strand break repair. *PLoS Genet.* **9**, e1003277 (2013).
21. H. Wang *et al*., CtIP maintains stability at common fragile sites and inverted repeats by end resection-independent endonuclease activity. *Mol. Cell* **54**, 1012–1021 (2014).
22. C. Zhu *et al*., Unrepaired DNA breaks in p53-deficient cells lead to oncogenic gene amplification subsequent to translocations. *Cell* **109**, 811–821 (2002).
23. X. S. Wang, B. J. Lee, S. Zha, The recent advances in non-homologous end-joining through the lens of lymphocyte development. *DNA Repair (Amst.)* **94**, 102874 (2020).
24. S. Rooney *et al*., Artemis and p53 cooperate to suppress oncogenic N-myc amplification in progenitor B cells. *Proc. Natl. Acad. Sci. U.S.A.* **101**, 2410–2415 (2004).
25. Y. Gao *et al*., A critical role for DNA end-joining proteins in both lymphogenesis and neurogenesis. *Cell* **95**, 891–902 (1998).
26. M. Nacht *et al*., Mutations in the p53 and SCID genes cooperate in tumorigenesis. *Genes Dev.* **10**, 2055–2066 (1996).
27. G. J. Vanasse *et al*., Genetic pathway to recurrent chromosome translocations in murine lymphoma involves V(D)J recombinase. *J. Clin. Invest.* **103**, 1669–1675 (1999).
28. O. Shoshani *et al*., Chromothripsis drives the evolution of gene amplification in cancer. *Nature* **591**, 137–141 (2020).
29. H. Tanaka, T. Watanabe, Mechanisms underlying recurrent genomic amplification in human cancers. *Trends Cancer* **6**, 462–477 (2020).
30. J. H. Brann, S. J. Firestein, A lifetime of neurogenesis in the olfactory system. *Front. Neurosci.* **8**, 182 (2014).
31. A. Kurimasa *et al*., Catalytic subunit of DNA-dependent protein kinase: Impact on lymphocyte development and tumorigenesis. *Proc. Natl. Acad. Sci. U.S.A.* **96**, 1403–1408 (1999).
32. C. Jhappan, H. C. Morse III, R. D. Fleischmann, M. M. Gottesman, G. Merlino, DNA-PKcs: A T-cell tumour suppressor encoded at the mouse scid locus. *Nat. Genet.* **17**, 483–486 (1997).
33. M. Gostissa *et al*., Long-range oncogenic activation of Igh-c-myc translocations by the Igh 3′ regulatory region. *Nature* **462**, 803–807 (2009).
34. Y. Ma, U. Pannicke, K. Schwarz, M. R. Lieber, Hairpin opening and overhang processing by an Artemis/DNA-dependent protein kinase complex in nonhomologous end joining and V(D)J recombination. *Cell* **108**, 781–794 (2002).
35. W. Jiang *et al*., Differential phosphorylation of DNA-PKcs regulates the interplay between end-processing and end-ligation during nonhomologous end-joining. *Mol. Cell* **58**, 172–185 (2015).
36. B. M. Lengsfeld, A. J. Rattray, V. Bhaskara, R. Ghirlando, T. T. Paull, Sae2 is an endonuclease that processes hairpin DNA cooperatively with the Mre11/Rad50/Xrs2 complex. *Mol. Cell* **28**, 638–651 (2007).
37. K. M. Trujillo, P. Sung, DNA structure-specific nuclease activities in the Saccharomyces cerevisiae Rad50*Mre11 complex. *J. Biol. Chem.* **276**, 35458–35464 (2001).
38. W. Wang, J. M. Daley, Y. Kwon, D. S. Krasner, P. Sung, Plasticity of the Mre11-Rad50-Xrs2-Sae2 nuclease ensemble in the processing of DNA-bound obstacles. *Genes Dev.* **31**, 2331–2336 (2017).
39. A. L. Bredemeyer *et al*., ATM stabilizes DNA double-strand-break complexes during V(D)J recombination. *Nature* **442**, 466–470 (2006).
40. B. S. Lee *et al*., Functional intersection of ATM and DNA-PKcs in coding end joining during V(D)J recombination. *Mol. Cell Biol.* **33**, 3568–3579 (2013).
41. J. Hu *et al*., Detecting DNA double-stranded breaks in mammalian genomes by linear amplification-mediated high-throughput genome-wide translocation sequencing. *Nat. Protoc.* **11**, 853–871 (2016).
42. U. Pannicke *et al*., Functional and biochemical dissection of the structure-specific nuclease ARTEMIS. *EMBO J.* **23**, 1987–1997 (2004).
43. X. Li, J. K. Tyler, Nucleosome disassembly during human non-homologous end joining followed by concerted HIRA- and CAF-1-dependent reassembly. *eLife* **5**, e15129 (2016).
44. J. Oh, L. S. Symington, Role of the Mre11 complex in preserving genome integrity. *Genes (Basel)* **9**, 589 (2018).
45. H. Chen *et al*., Sae2 promotes DNA damage resistance by removing the Mre11-Rad50-Xrs2 complex from DNA and attenuating Rad53 signaling. *Proc. Natl. Acad. Sci. U.S.A.* **112**, E1880–E1887 (2015).
46. G. Wu, W. H. Lee, CtIP, a multivalent adaptor connecting transcriptional regulation, checkpoint control and tumor suppression. *Cell Cycle* **5**, 1592–1596 (2006).
47. Z. You, J. M. Bailis, DNA damage and decisions: CtIP coordinates DNA repair and cell cycle checkpoints. *Trends Cell Biol.* **20**, 402–409 (2010).
48. O. Barton *et al*., Polo-like kinase 3 regulates CtIP during DNA double-strand break repair in G1. *J. Cell Biol.* **206**, 877–894 (2014).
49. T. Y. Yu, M. T. Kimble, L. S. Symington, Sae2 antagonizes Rad9 accumulation at DNA double-strand breaks to attenuate checkpoint signaling and facilitate end resection. *Proc. Natl. Acad. Sci. U.S.A.* **115**, E11961–E11969 (2018).
50. B. Shiotani, L. Zou, Single-stranded DNA orchestrates an ATM-to-ATR switch at DNA breaks. *Mol. Cell* **33**, 547–558 (2009).
51. L. Pasqualucci *et al*., AID is required for germinal center-derived lymphomagenesis. *Nat. Genet.* **40**, 108–112 (2008).
52. R. C. Rickert, J. Roes, K. Rajewsky, B lymphocyte-specific, Cre-mediated mutagenesis in mice. *Nucleic Acids Res.* **25**, 1317–1318 (1997).
53. D. Dominguez-Sola *et al*., Non-transcriptional control of DNA replication by c-Myc. *Nature* **448**, 445–451 (2007).
54. B. A. Helmink *et al*., H2AX prevents CtIP-mediated DNA end resection and aberrant repair in G1-phase lymphocytes. *Nature* **469**, 245–249 (2011).
55. E. P. Mimitou, L. S. Symington, Ku prevents Exo1 and Sgs1-dependent resection of DNA ends in the absence of a functional MRX complex or Sae2. *EMBO J.* **29**, 3358–3369 (2010).
56. Z. E. Karanjawala *et al*., The embryonic lethality in DNA ligase IV-deficient mice is rescued by deletion of Ku: Implications for unifying the heterogeneous phenotypes of NHEJ mutants. *DNA Repair (Amst.)* **1**, 1017–1026 (2002).
57. J. Bartkova *et al*., Oncogene-induced senescence is part of the tumorigenesis barrier imposed by DNA damage checkpoints. *Nature* **444**, 633–637 (2006).
58. J. C. Saldivar, D. Cortez, K. A. Cimprich, The essential kinase ATR: Ensuring faithful duplication of a challenging genome. *Nat. Rev. Mol. Cell Biol.* **18**, 622–636 (2017).

59. N. L. Mozaffari, F. Pagliarulo, A. A. Sartori, Human CtIP: A 'double agent' in DNA repair and tumorigenesis. *Semin. Cell Dev. Biol.* **113**, 47–56 (2020).
60. C. R. Reczek *et al*., The DNA resection protein CtIP promotes mammary tumorigenesis. *Oncotarget* **7**, 32172–32183 (2016).
61. Y. Gao *et al*., A targeted DNA-PKcs-null mutation reveals DNA-PK-independent functions for KU in V(D)J recombination. *Immunity* **9**, 367–376 (1998).
62. T. Jacks *et al*., Tumor spectrum analysis in p53-mutant mice. *Curr. Biol.* **4**, 1–7 (1994).
63. A. L. Kovalchuk *et al*., Burkitt lymphoma in the mouse. *J. Exp. Med.* **192**, 1183–1190 (2000).
64. M. Milanovic *et al*., FATC domain deletion compromises ATM protein stability, blocks lymphocyte development, and promotes lymphomagenesis. *J. Immunol.* **206**, 1228–1239 (2021).
65. D. Menolfi *et al*., Kinase-dead ATR differs from ATR loss by limiting the dynamic exchange of ATR and RPA. *Nat. Commun.* **9**, 5351 (2018).